U.S. Department of Commerce
National Oceanic and Atmospheric Administration
National Weather Service
National Centers for Environmental Prediction
5830 University Research Court
College Park, MD 20740-3818

Office Note 500
https://doi.org/10.25923/4nhy-x681

A FORMULATION OF THE DECAD ALGORITHM USING THE SYMMETRIES OF THE GALOIS FIELD, $GF(16)$

R. James Purser*
IM Systems Group, Rockville, Maryland

January 30, 2020

This is an unreviewed manuscript, primarily intended for informal exchange of information among the NCEP staff members

* email: jim.purser@noaa.gov

Abstract

A companion study showed how a Galois field, $GF(8)$, and its symmetries could be exploited to simplify the formal speicification of the 'Hexad Algorithm' by which a symmetric positive-definite second moment 'aspect tensor' in three dimensional can always by decomposed into six one-dimensional aspect tensors acting along generalized grid lines. The present study extends this technique to four dimensions, where the symmetric aspect tensor possesses ten independent components and where it is therefore the aim of the corresponding 'Decad' algorithm to produce ten generalized grid line generators, conforming collectively to a fixed pattern of linear relationships sufficient to ensure the set's uniqueness in each case, and their corresponding nonnegative 'aspect weights'. In four dimensions, this is a nontrivial task owing to several additional geometrical and algebraic complexities not present in lower dimensions, as we will be discussed. Foremost amongst these is the fact that the natural and most symmetrical decomposition of a generic aspect tensor into rank-one components along generalized grid lines leads, in the majority of cases, to a set of twelve (not ten) lines in a configuration with a high degree of symmetry. As in the three-dimensional case, the appropriate Galois field and associated finite projective geometry provides the means to distinguish and label the line directions, and thereby enables the high order of symmetry of the recovered line sets to be broken in a systematic and repeatable way. In this way a true 'decad' of ten lines directions can be unambiguously chosen and canonically orientated in every case of valid aspect tensor. The appropriate Galois field in this case is $GF(16)$, most naturally represented by 4-vectors of binary digits, and its associated finite projective space is the three-dimensional one, $PG(3, 2)$.

1. Introduction

This note extends the discussion of the companion office note (Purser, 2020), where the three-dimensional (3D) Hexad extension of the two-dimensional (2D) Triad algorithm was described, in order to deal with the much more complicated four-dimensional (4D) case of the 'Decad' algorithm for synthesizing anisotropic quasi-Gaussian covariance components by line filters. The original line filters were the so-called 'recursive filters' developed by Purser and McQuigg (1982), Hayden and Purser (1995) for empirical analyses, and by Wu et al. (2002), and Purser et al. (2003a, b) for variational analysis with the option of employing fully anisotropic covariances based on the Triad or Hexad methods in the 2D and 3D cases. The original motivation for this study was to see whether the clear advantages that accrued from the adoption into the Hexad's algorithmic strucure of the symmetries of the Fano plane, or $PG(2,2)$ finite projective space, would carry over into the space-time domain discretized by a 4D lattice, and allow the resolution of some long-standing technical obstacles to a satisfactory generalization, in this larger gridded space, of the Hexad algorithm to the analogous 4D Decad algorithm. By having, for the first time, a highly efficient means for convolving or smoothing weighted observational data with effective space-time covariances that can be stretched in the time dimension along Lagrangian trajectories as well as exhibiting the usual spatially distortions of a controlled imposed anisotropy, an additional motivating hope is that, in the not too distant future, we shall be able to emulate the proven successes of the anisotropic analyses of the 2D and 3d Real-Time Mesoscale Analysis (RTMA; for example, de Pondeca 2011) to some form of fully 4D 'nowcasting' extension into the temporal domain. This new capability will enable a greater temporal consistency within each analysis as compared against its input observations collected at different times, implying an improved dynamical consistency overall. But it also provides the means to extrapolate these temporally evolving smooth analysis increments for at least a short period into the future where their skill presumably persists, thereby avoiding the relatively exorbitant cost incurred by initializing and running a full dynamical model every time.

We say a few words about the technical obstacles, mentioned above, that have hitherto precluded a simple generalization of the anisotropic covariance algorithms to four dimensions. In constrast to the 3D Hexad case, the 4D decomposition does not naturally result in a uniform set of essentially congruent polytopes (a '*polytope*' is a generalization of the the concept of a 'polygon' or 'polyhedron' to *any* finite number of dimensions). To explain how the actual decomposition emerges (this argument will be valid in *any* number of dimensions), consider the *tensor image* in the space of $N(N+1)/2$ independent components of the outer-product tensor of a *generator* of the regular lattice in N dimensions. (A generator is an irreducible integer N-vector, which points along some generalized line of the grid or lattice.) The opposite, or negative, of a generator is obviously also a valid generator; it identifies the same line and has the same tensor image. The tensor image is some integer vector in the higher-dimensioned *aspect space*, and the set of *all* such generators has a *convex hull* in that space (a convex hull of a set of points is defined as the set of all points that can be identified with a non-negative weighted mean of members of this set). The boundary of the convex hull forms a polyhedral *convex shell* – a hypersurface of dimension one less (i.e., $(N^2+N-2)/2$) than the dimensionality of the aspect space itself. In the cases where $N=2$ or $N=3$, the polytope elements that form this shell are simplexes in 2 and 5 dimensions, which we can call '3-simplexes' (or just triangles) and '6-simplexes', after the numbers of vertices these simplexes possess. But the case in 4D is complicated by the fact that the aspect space 9D convex shell bounding the convex hull of the tensor images of the generators comprises *two* distinct types of polytope: the first kind, which we conveniently refer to as the '*A-topes*', are indeed 10-simplexes as we might naively expect, but a second type of polytope is an object with 12 vertices, which we refer to as a '*B-tope*'. (In higher dimensions, $N > 4$, we should not be surprised that the geometrical description becomes even more complicated.)

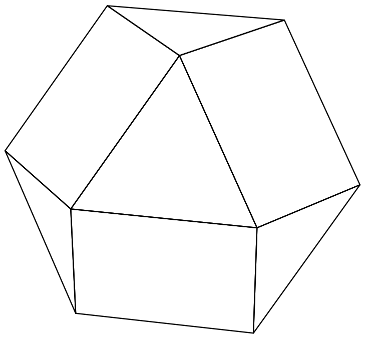

Figure 1. The Archimedean solid known as the 'cuboctahedron'.

One of the tasks required in order to develop a viable 'Decad' algorithm is to systematically dissect the B-topes into smaller fragments that are each a 10-simplex, because our aim is to synthesize any given aspect tensor in terms of line smoothers acting along *only* ten lines – the lines associated with the set of possible *preimages* of the vertices of the 10-simplexes. In the Hexad case, $N = 3$, the preimages of one of the six vertices of the 6-simplex were the mutually-opposite pair of valid generators which defined one of the smoothing lines (recall, we usually do not distingush between a generator and its negative since they imply the same tensor image; the exception is when we need to perform linear operations with these generators). The set of six pairs of the preimages of the 6-simplex (i.e., 12 integer 3-vectors) always had a convex hull in the form of a squashed cuboctahedron, as depicted in Fig. 1. In $N = 2$, the Triad algorithm, the corresponding shape of the convex hull of the three pairs of preimages of the 3-simplex, was a hexagon. In our $N = 4$ case, the 20 possible preimages of the ten vertices of the 10-simplex A-tope form the vertices of a 4D polytope which we can loosely think of as the 4D analog of the previously discussed hexagon and cuboctahedron; in its most isotropic (unsquashed) stretching, its boundary hypersurface is composed of 20 square-sided triangular prisms capped at their ends by ten tetrahedra. As in the 2D and 3D cases, this polytope is the convolution of a simplex with its dual. Alternatively, just as the hexagon can be regarded as the triangle with its vertices planed off, and the cuboctahedron regarded as the tetrahedron with its vertices *and* edges sufficiently planed off, our 4D object can be obtained by sufficiently planing ('runcinating') vertices, edges and planes of the 5-simplex and, for this reason, it is sometimes referred to as the '*runcinated 5-cell*'. The 24 preimages of the vertices of the B-tope, when linearly transformed to their most isotropic configuration, form the vertices of a well-known 4D regular polytope, the so-called '*24-cell*'.

We showed in the companion note that the simplest construction of the 3D Hexad algorithm resulted by exploiting the symmetries imposed by tagging the lattice generators with the non-null elements of the Galois field, $GF(8)$. Veblen and Bussey (1906) introduced the now standard classification of the finite projective geometries associated with Galois Fields, denoting the particular geometry of dimension d over the individual entries of a Galoid field $GF(n)$ by '$PG(d,n)$'. The seven non-null element of $GF(8)$, by which the Hexad algorithm is constructed in its most symmetric form, form seven '*triads*' (with vector sums being zero) which we can associate with the projective plane of Fano (1892) and which, by the notation of Velblen and Bussey, is denoted $PG(2,2)$. The indices of any Galois field $GF(p^n)$ (effectively the '*logarithms*' of the Galois field elements) can be taken to run from 0 through p^n-2 and to obey modular arithmetic, that is, addition modulo-(p^n-1), corresponding to (commutative) multiplication of the corresponding field elements. We also find that modulo-(p^n-1) multiplication by some k co-prime to (p^n-1) of the logarithms of the Galois elements, in other words, raising each element to the power k, induces a special kind of '*automorphism*' – a structure-preserving re-labeling of the elements of the projective geometry associated with that Galois field. These are properties that we exploit as we try to seek formulations of the Hexad and Decad algorithm that exhibit as much formal symmetry as possible. The cyclic indices of the Galois field non-null elements are informally referred to as '*colors*' in the context of the Triad, Hexad and now the Decad algorithms. In these 'chromatic' polyad algorithms the colors were originally introduced to label, globally, the generator directions of the line filters so that, by grouping and performing all the operations of each successive color in order, we can guarantee the avoidance of any filtering conflict or tangle implied by one line of filtering running across another before either filtering operation is completed. It was only later that it was realized that, besides its advantage in providing a convenient line-labeling scheme, the Galois field concept could be advantageously exploited for it arithmetic attributes as well.

The obvious chromatic extension of any decad algorithm would involve the 15 *colors* as-sociated with the non-null elements of the Galois field, $GF\,(16)$. These 15 non-null elements are also equivalent to the 15 '*points*' of the three-dimensional finite projective space, $PG(3,\,2)$ discussed in the next section. When we check, we indeed find that the colors of each of the pairs of preimages of the vertices of the 10-simplex A-tope, and the 12-pointed B-tope, are distinct in both cases, so this Galois field is the right one to use to order the set of line operations so that successive filtering operations cannot interfere with each other. In the next section we construct the elements of the particular integer 4-vector representation of GF (16) that we shall be adopting, and describe the associated finite geometry $PG(3,\,2)$. Sections 3 and 4 will focus on the geometrical aspects and organization of the Decad algorithm, and the dissection of the B-topes into the required sub-simplexes. Section 5 contains a discussion and conclusions.

2. A representation of $GF(16)$ and the associated geometry, PG(3,2)

We can think of the Galois field $GF(2^4)$ as the coefficients, restricted to the residual prime field, modulo-2, of polynomials, $b_0+b_1z+b_2z^2+b_3z^3$, with a polynomial modulus, $P(z)=1+z+z^4$, which means that all the polynomials can be reduced to just the set of up to degree-3 with just a quartet (b_0,b_1,b_2,b_3) of binary digit components. Apart from the null polynomial, which is not of interest to us, we can start with the polynomial, $g_0=1\equiv(1,0,0,0)$, and derive the rest by multiplying successively by $z \equiv (0, 1, 0, 0)$ with the above modulus conditions. The resulting cyclic series of the elements g_k are explicitly listed in Table 1.

TABLE 1. A representation of the non-null elements of the Galois field, $GF(16)$ as a cyclic sequence of 15 binary 4-vectors, that we can take as the coefficients of a cubic polynomial in z.

D	g_0	g_1	g_2	g_3	g_4	g_5	g_6	g_7	g_8	g_9	g_{10}	g_{11}	g_{12}	g_{13}	g_{14}
b_0	1	0	0	0	1	0	0	1	1	0	1	0	1	1	1
b_1	0	1	0	0	1	1	0	1	0	1	1	1	1	0	0
b_2	0	0	1	0	0	1	1	0	1	0	1	1	1	1	0
b_3	0	0	0	1	0	0	1	1	0	1	0	1	1	1	1

The associative and commutative ('Abelian') laws of the operation of multiplication, which apply to polynomials with or without modular-arithmetic clauses, are inherited by the abstract elements g_k of $GF(2^4)$, as are additions on the understanding that components are added modulo-2. So, having established how these elements add and multiply, we can dispense with any further consideration of the particular 'polynomial' interpretation we adopted to motivate their formal creation. From here on, we shall regard the elements g_k as either binary 4-vectors, or simply use their indices k as convenient labels of the objects (grid lines or their line generators) that we map to them.

Unlike in the cases, $N = 2$ and $N = 3$, where the Galois fields had sets of non-null elements numbering prime numbers, (3 for the Triad algorithm, 7 for the Hexad algorithm), now, with $N = 4$, the 15 non-null elements of $GF(16)$ means that the cyclic group C_{15} that the elements conform to under multiplication, factors into primes, $15 = 3 \times 5$. This has complicating consequences in the construction of the Decad algorithm, as we shall find in the following sections.

In the $PG(3, 2)$ geometry, the 'lines' comprise all the triads of the non-null elements of GF(16) that sum to zero vectors of their representation. For brevity, we write the ordered triad $\{g_i, g_j, g_k\}$ such that $g_i + g_j + g_k = \mathbf{0}$ as simply (i, j, k). These form the 'lines' of $PG(3, 2)$. There are 35 such lines, which, in our chosen representation, comprise the following triads of the 15 points:

$$\mathcal{L}_k = (0, 2, 8) + (k, k, k), \quad (\text{mod } 15) \qquad k = 0, \dots 14 \tag{2.1a}$$

$$\mathcal{L}'_k = (0, 1, 4) + (k, k, k), \quad (\text{mod } 15) \qquad k = 0, \dots 14 \tag{2.1b}$$

$$\mathcal{L}''_k = (0, 5, 10) + (k, k, k), \qquad k = 0, \dots 4. \tag{2.1c}$$

In this way, every pair of 'points' belongs to a unique 'line' that also contains one other point. Each plane comprises the union of a point, a line not including this point, and the three additional points belonging to the three lines between the original point and the points of the original line, thus making seven points in all. There are 15 planes which, in our representation, comprise the points:

$$\mathcal{P}_k = (0, 1, 2, 4, 5, 8, 10) + (k, k, k, k, k, k, k), \quad (\text{mod } 15) \qquad k = 0, \dots 14. \tag{2.2}$$

Each plane contains seven lines:

$$\mathcal{P}_k = \bigcup\{\mathcal{L}_k, \mathcal{L}_{k+2}, \mathcal{L}_{k+8}, \mathcal{L}'_k, \mathcal{L}'_{k+1}, \mathcal{L}'_{k+4}, \mathcal{L}''_k\}, \qquad k = 0, 14, \tag{2.3}$$

where the indices of $\mathcal{L}$ and $\mathcal{L}'$ are treated modulo-15 and those of $\mathcal{L}''$ are treated modulo-5. Each pair of planes intersects at a unique line, and each plane is itself a version of the Fano plane with undirected lines.

Our use of the Fano plane geometry in the construction of the 3D Hexad algorithm used the special variant in which the Fano lines were directed, and these directions (or cyclic orderings of the points) were preserved by the '*squaring automorphism*' of the structure defined by multiplying ×2 modulo-7, the logarithms, or 'colors' of each of the Galois non-null elements. The larger geometry of $PG(3,2)$ does not lend itself to the consistent use of directed lines in the same way; for example, the operation of squaring, modulo-15, necessarily leads to the reversal of the directions of some of the lines. Nevertheless, the four automorphisms induced by applying formal powers of $1 \equiv 2^0$, $2 \equiv 2^1$, $4 \equiv 2^2$, and $8 \equiv 2^3$, do continue to map lines to lines, and therefore map our planes to planes as well. Multiplications by other numbers do not preserve the integrity of all of the lines, and will play no role in the further development. Note that $16 \equiv 2^4 \equiv 1$ in modulo-15 arithmetic, so this cycle of consecutive squaring automorphisms is complete in four steps; in other words, this particular group of automorphisms is a representation of the cyclic group, C_4. The restricted group of automorphisms, which we call $\mathrm{Aut}^+\{PG(3,2)\}$, generated by arbitrary combinations of 'squaring' and 'multiplying' the elements of associated $GF(16)$ is closed at $|\mathrm{Aut}^+\{PG(3,2)\}| = 60$ elements. As in the case for the Hexad algorithm, this is technically a semi-direct product,

$$\mathrm{Aut}^+\{PG(3,2)\} = C_{15} \rtimes C_4, \tag{2.4}$$

with C_{15} being the '*normal*' subgroup of the pair (right and left cosets being the same, as discussed in the companion note). A notable difference from the 3D case is that the 'lines' of $PG(3,2)$ are not all images of one another under the action of elements of $\mathrm{Aut}^+\{PG(3,2)\}$, since the lines of $\mathcal{L}''$ form one invariant set, while those of $\mathcal{L}$ and $\mathcal{L}'$ form another. Nevertheless, this group contains enough symmetry to make it advantageous to formulate the Decad algorithm in a way that conforms to these symmetries as much as possible. The full group, $\mathrm{Aut}^+\{PG(3,2)\}$, of *all* possible automorphisms of the finite geometry is very much larger, in this case $|\mathrm{Aut}\{PG(3,2)\}| = 20160$, so we are only actively tapping into a very special subgroup of this larger group of structural symmetries of $PG(3,2)$ as we proceed.

3. Lattice generators and symmetries

We have referred to the 9-dimensional tensor-image polytopes as 'A-topes' when they possess 10 vertices, and 'B-topes' when they possess 12; we shall refer to the preimages of the A-topes as 'decads', comprising 10 pairs of the generators, and the preimages of the B-topes as 'dodecads', comprising 12 opposing pairs of generators, although in the presentations that follow, we generally exhibit only one member of each pair, and shall be careful also to choose these representative members in such a way that certain linear relationships amongst them, when they are framed in a standard ordering, are preserved.

The most symmetrical presentations of lattice polytopes are often found by using a super-lattice, either of higher dimensions, or possessing additional intermediate points, of which the lattice used in the practical computation constitutes a sub-lattice. In the cases of the polytopes that naturally generalize the 2D hexagon of the Triad algorithm, and the 3D cuboctahedron of the Hexad algorithm, i.e., that are the convolutions of a minimal lattice simplex with its geometrical inversion, it is generally the case that a simple lattice in a dimension one higher than the intended dimension actually allows the most symmetrical presentation, by placing all the involved points on the obliquely angled plane through the origin on which all the integer lattice coordinates sum to zero. The same method also works for the decads (A-tope preimages), but does not help for the dodecads. We first consider the decads.

A systematic construction of one member of each of the ten pairs of mutually-opposite generators of an idealized decad could produce the following possible tableau (which generalizes in the obvious way to any number of dimensions). Recall that the decad resides in an oblique 4-dimensional subspace lattice, but is here exhibited in five dimensions (temporarily) in order to reveal the generic pattern of its most symmetrical presentation:

$$\left\{ \begin{array}{rrrr|rrr|rr|r} 1 & 1 & 1 & 1 & 0 & 0 & 0 & 0 & 0 & 0 \\ -1 & 0 & 0 & 0 & 1 & 1 & 1 & 0 & 0 & 0 \\ 0 & -1 & 0 & 0 & -1 & 0 & 0 & 1 & 1 & 0 \\ 0 & 0 & -1 & 0 & 0 & -1 & 0 & -1 & 0 & 1 \\ 0 & 0 & 0 & -1 & 0 & 0 & -1 & 0 & -1 & -1 \end{array} \right\} . \tag{3.1}$$

But we can rearrange these column 5-vectors, possibly switching some of their signs, and organize them into two related cycles of five, a set 'G' and a set 'H', each possessing a sign and indexed j from 0 to 4, in order to bring out more obviously some of the inherent latent symmetry of this decad:

$$\mathrm{DECAD}(j) = \begin{array}{rrrrrcrrrrr} j=0 & 1 & 2 & 3 & 4 & \quad & j=5 & 6 & 7 & 8 & 9 \\ \boldsymbol{G}_0 & \boldsymbol{G}_1 & \boldsymbol{G}_2 & \boldsymbol{G}_3 & \boldsymbol{G}_4 & & \boldsymbol{H}_0 & \boldsymbol{H}_1 & \boldsymbol{H}_2 & \boldsymbol{H}_3 & \boldsymbol{H}_4 \\ 1 & 0 & -1 & 0 & 0 & & 0 & 0 & 0 & 1 & -1 \\ -1 & 0 & 0 & 1 & 0 & & 0 & 1 & -1 & 0 & 0 \\ 0 & 1 & 0 & -1 & 0 & & -1 & 0 & 0 & 0 & 1 \\ 0 & -1 & 0 & 0 & 1 & & 0 & 0 & 1 & -1 & 0 \\ 0 & 0 & 1 & 0 & -1 & & 1 & -1 & 0 & 0 & 0 \end{array} . \tag{3.2}$$

Clearly, the sums of the G- and H- 'pentads' separately come to zero. If we take the indices modulo-5, we find that the following 'triad' relationships hold:

$$\boldsymbol{G}_{j-1} + \boldsymbol{H}_j + \boldsymbol{G}_{j+1} \;=\; \mathbf{0} \tag{3.3a}$$
$$\boldsymbol{H}_{j-2} + \boldsymbol{G}_j + \boldsymbol{H}_{j+2} \;=\; \mathbf{0}, \tag{3.3b}$$

as well as the 'tetrad' relationships:

$$\boldsymbol{G}_k + \boldsymbol{H}_k + \boldsymbol{H}_{k+1} + \boldsymbol{H}_{k+4} \;=\; \mathbf{0} \tag{3.4a}$$
$$\boldsymbol{G}_k - \boldsymbol{G}_{k+1} - \boldsymbol{H}_{h+2} + \boldsymbol{H}_{k+4} \;=\; \mathbf{0} \tag{3.4b}$$
$$\boldsymbol{G}_k + \boldsymbol{G}_{k+1} + \boldsymbol{G}_{k+3} - \boldsymbol{H}_{k+3} \;=\; \mathbf{0}. \tag{3.4c}$$

But to see the full range of symmetries it is perhaps useful to show a graphical representation of these generators, together with their opposites (negatives), identified, in two distinct but dually-related ways, with the faces of a pair of regular icosahedra. We can also, arbitrarily,

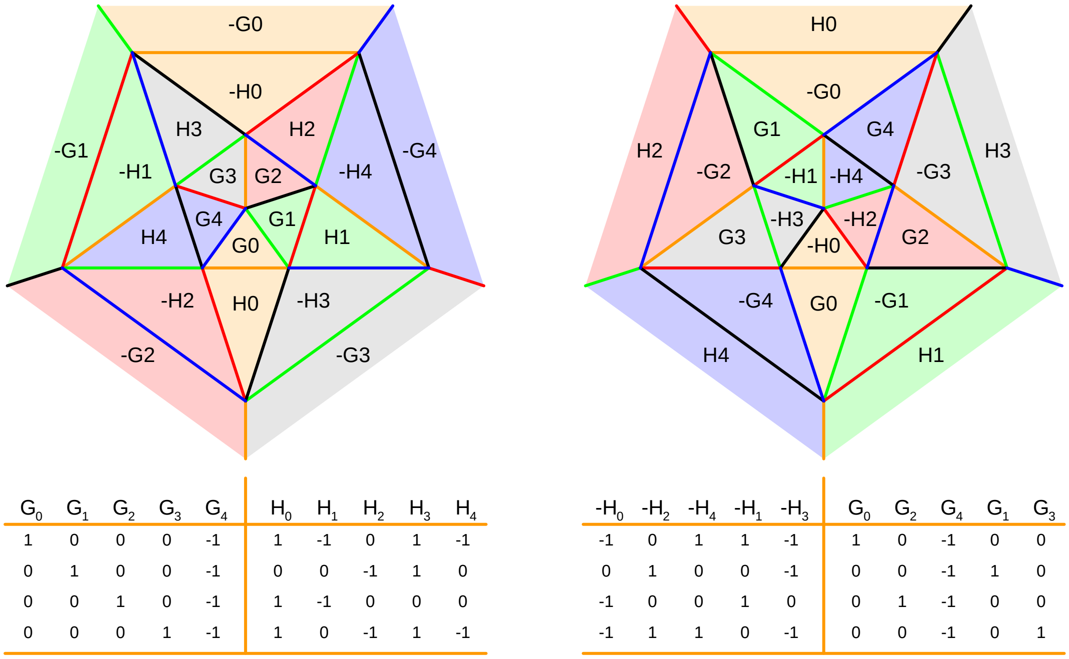

G_0	G_1	G_2	G_3	G_4	H_0	H_1	H_2	H_3	H_4
1	0	0	0	-1	1	-1	0	1	-1
0	1	0	0	-1	0	0	-1	1	0
0	0	1	0	-1	1	-1	0	0	0
0	0	0	1	-1	1	0	-1	1	-1

$-H_0$	$-H_2$	$-H_4$	$-H_1$	$-H_3$	G_0	G_2	G_4	G_1	G_3
-1	0	1	1	-1	1	0	-1	0	0
0	1	0	0	-1	0	0	-1	1	0
-1	0	0	1	0	0	1	-1	0	0
-1	1	1	0	-1	0	0	-1	0	1

Figure 2. The identification of the signed-generators of the decad of (3.5) with the faces of a related pair of icosahedra. Alternative pentads, summing to zero, are found around every vertex, and the triads are found as the elements surrounding each triangular face.

take the first four members of the G-pentad as the 4D lattice basis vectors, so that, relative to them, the coordinates of the G and H pentads become:

$$\mathrm{DEC0}(j) = \begin{array}{rrrrrcrrrrr} j=0 & 1 & 2 & 3 & 4 & & j=5 & 6 & 7 & 8 & 9 \\ \boldsymbol{G}_0 & \boldsymbol{G}_1 & \boldsymbol{G}_2 & \boldsymbol{G}_3 & \boldsymbol{G}_4 & & \boldsymbol{H}_0 & \boldsymbol{H}_1 & \boldsymbol{H}_2 & \boldsymbol{H}_3 & \boldsymbol{H}_4 \\ 1 & 0 & 0 & 0 & -1 & & 1 & -1 & 0 & 1 & -1 \\ 0 & 1 & 0 & 0 & -1 & & 0 & 0 & -1 & 1 & 0 \\ 0 & 0 & 1 & 0 & -1 & & 1 & -1 & 0 & 0 & 0 \\ 0 & 0 & 0 & 1 & -1 & & 1 & 0 & -1 & 1 & -1 \end{array} . \tag{3.5}$$

Figure 2 sketches how we might map these decad vertices, of both signs, to the 20 faces of an icosahedron in two distinct but complementary ways. In the left panel, the ‘G’ generators with positive signs map to the inner ring, while the ‘H’ generators with positive signs map to the ring of corresponding neighbors of the inner ‘Gs’. The rotations and reflections of the icosahedron offer us many alternative inner rings from which other equally valid G-sets can be constructed, together with the corresponding H-sets taken from the ring of faces one step farther out. These alternative representations rotate the decad into a new presentation, but the linear relationships among the newly labeled G and H sets are still those of (3.5). This means the basis formed from the first four vectors is always enough to define the rest of the full decad of generators. An additional range of symmetries of the decads is obtained by consideration also of the alternatively arranged icosahedron of the right panel, which we can also rotate and reflect to provide other valid choices for the G-set and H-set in the same manner. In all, these options provide 240 different ways of representing the same decad. We can ask: does this exhaust the symmetries of the decad? Recalling that the convex hull polytope of the decad in its most symmetric form, the runcinated 5-cell, is Archimedian (vertex-symmetric) and contains on its boundary hyper-surface ten congruent regular tetrahedra, we deduce, from the 24 rotation and reflection symmetries of each tetrahedron, that the total number of symmetries of the decad amount to $24 \times 10 = 240$. Thus, since the symmetries of a single icosahedron amount to 120, the identification of the symmetries with the *pair* of icosahedrons of Fig. 2 is a complete and faithful one. For example, an alternative but equivalent representation of the decad of (3.5) is obtained by a rotation (and a reflection) of the icosahedron of the right panel of Fig. 2 that implies the new inner ring of elements and their neighbors can be relabeled:

$$\begin{aligned} \{\boldsymbol{G}'_0, \boldsymbol{G}'_1, \boldsymbol{G}'_2, \boldsymbol{G}'_3, \boldsymbol{G}'_4 | \boldsymbol{H}'_0, \boldsymbol{H}'_1, \boldsymbol{H}'_2, \boldsymbol{H}'_3, \boldsymbol{H}'_4\} \qquad & = \\ \{\boldsymbol{G}_2, -\boldsymbol{G}_1, \boldsymbol{G}_0, -\boldsymbol{H}_0, -\boldsymbol{H}_2| - \boldsymbol{G}_3, \boldsymbol{H}_1, -\boldsymbol{G}_4, -\boldsymbol{H}_3, -\boldsymbol{H}_4\}. & \end{aligned} \tag{3.6}$$

This happens to be the standard presentation chosen to initialize the final algorithm, and we will refer to it later.

Unlike in the case of Hexad algorithm, we find that we cannot, without unduly complicating the algorithm, restrict our representations of the decads to a single chirality (and the same applies to the dodecads). We also note that reversing the signs of all the components of all components of vectors in 4D does not change the chirality, so a feature of the decad algorithm that we must get used to is that the generator vectors provided will not consistently be of the same sign from one location to the next, even when they are intended to indicate the same line. Next, we consider the dodecads.

In the case of the dodecads (preimages of the 12-vertex B-topes) the most symmetrical presentation is found in the 4D equivalent of a 'body-centered cubic' simple lattice, which means that we can take the union of one orthogonal lattice of two-unit spacing (all coordinates even integers) together with the parallel congruent interlaced lattice of coordinates that are only odd integer entries. In that case, a representative from each opposing generator pair, in this most symmetrical presentation, might be chosen to be the twelve column vectors of the tableau (3.7), where they are arranged in three distinct quartets. By analogy to the sub-categories of cards in a deck, we shall refer to these quartets as '*suits*' and arbitrarily label them $S^{(0)}$, $S^{(1)}$ and $S^{(2)}$, or just 'suit-0', etc., when there is no ambiguity. This categorization is intrinsic to the combinatorial structure of the dodecads (although the labels are not) since the group of 1152 symmetries of the 24-cell unfailingly maintains the integrity of each of these quartets. Geometrically, the four pairs of opposing vectors of a single suit define the eight vertices of an orthoplex (the dual to the hypercube). Also, the eight pairs of opposing vectors of any *two* of the suits define the 16 vertices of the hypercube itself.

$$\begin{array}{l} \mathrm{DODEC0}(j) = \\ \begin{array}{rrrrcrrrrcrrrr} j=0 & 1 & 2 & 3 & & j=4 & 5 & 6 & 7 & & j=8 & 9 & 10 & 11 \\ \boldsymbol{S}^{(0)}_0 & \boldsymbol{S}^{(0)}_1 & \boldsymbol{S}^{(0)}_2 & \boldsymbol{S}^{(0)}_3 & & \boldsymbol{S}^{(1)}_0 & \boldsymbol{S}^{(1)}_1 & \boldsymbol{S}^{(1)}_2 & \boldsymbol{S}^{(1)}_3 & & \boldsymbol{S}^{(2)}_0 & \boldsymbol{S}^{(2)}_1 & \boldsymbol{S}^{(2)}_2 & \boldsymbol{S}^{(2)}_3 \\ 2 & 0 & 0 & 0 & & -1 & 1 & 1 & 1 & & -1 & -1 & -1 & -1 \\ 0 & 2 & 0 & 0 & & -1 & 1 & -1 & -1 & & 1 & 1 & -1 & -1 \\ 0 & 0 & 2 & 0 & & -1 & -1 & 1 & -1 & & 1 & -1 & 1 & -1 \\ 0 & 0 & 0 & 2 & & -1 & -1 & -1 & 1 & & 1 & -1 & -1 & 1 \end{array} \end{array} \tag{3.7}$$

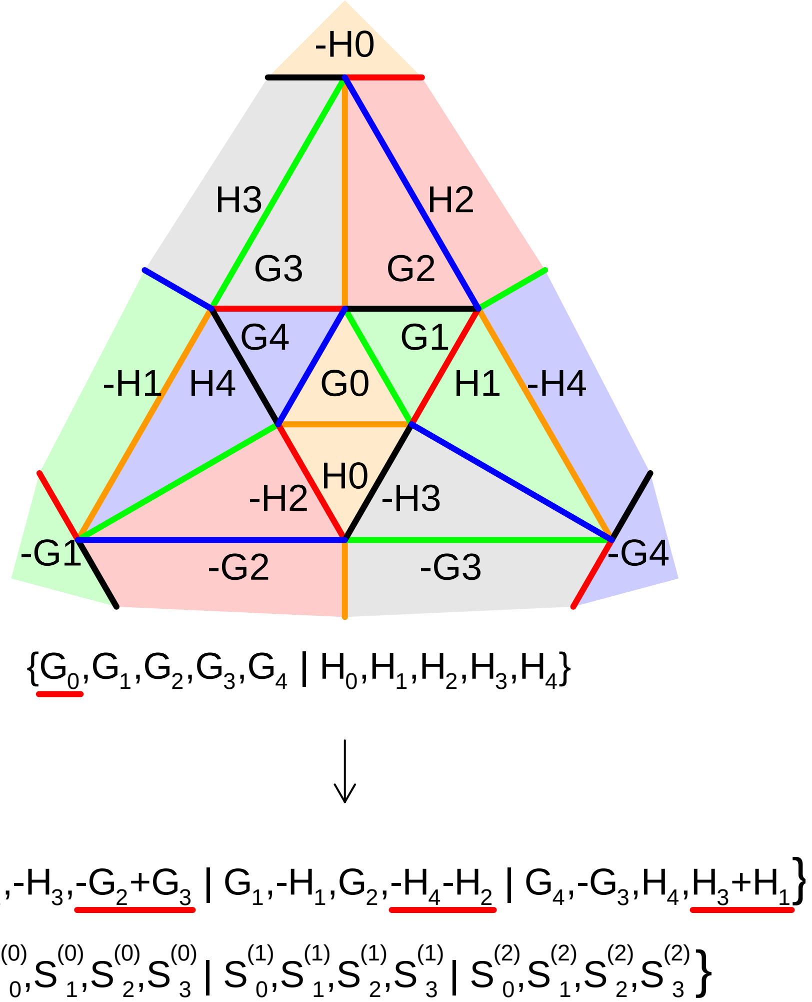
-H0
H3
H2
G3
G2
G4
G1
-H1
H4
G0
H1
-H4
H0
-H2
-H3
-G1
-G2
-G3
-G4
$\{\underline{G_0},G_1,G_2,G_3,G_4 \mid H_0,H_1,H_2,H_3,H_4\}$
$\downarrow$
$\{H_0,H_2,-H_3,\underline{-G_2+G_3} \mid G_1,-H_1,G_2,\underline{-H_4-H_2} \mid G_4,-G_3,H_4,\underline{H_3+H_1}\}$
$= \{S^{(0)}_0,S^{(0)}_1,S^{(0)}_2,S^{(0)}_3 \mid S^{(1)}_0,S^{(1)}_1,S^{(1)}_2,S^{(1)}_3 \mid S^{(2)}_0,S^{(2)}_1,S^{(2)}_2,S^{(2)}_3\}$

Figure 3. A geometrical representation of a generic transition from a decad to the neighboring dodecad, showing the three-fold symmetry of the transition rule. In the case illustrated, the generator $\boldsymbol{G}_0$ is retired, and three new generators are recruited, which become named $S_3^{(0)}$, $S_3^{(1)}$ and $S_3^{(2)}$ after the other nine are renamed in accordance to the pattern for dodecads, as shown. By rotating this icosahedral representation we deduce the transition rules involved in the retirement of any of the ten generators by applying the rules implied by the application of the same pattern used here.

Treated as a 4×10 matrix, the submatix of DEC0 of (3.5) formed by its first four columns is the identity matrix, so the whole of DEC0 can be used to complete *any* decad from a 'basis' given by its first four generators (with attention paid to their mutually-consistent signs) by multiplying on the right by *matrix* DEC0. Analogously, treated as a 4×12 matrix, the submatrix of DODEC0 of (3.7) formed by its first four columns is *twice* the identity. But, as with the decads, the dodecads can also be completed from only their first 'basis' vectors, except we must multiply the basis on the right by DODEC0 and divide the result by two to get the final tableau representing the completed dodecad.

A careful geometrical analysis reveals that each A-tope only has B-topes for neighbors (the converse is not true, though). We can use the icosahedral representations to illustrate schematically how a transition occurs between an A-tope and its neighboring B-tope. In such a transition, the A-tope loses one generator pair, which, by suitable relabeling according to the valid symmetries we have discussed, we can identify with a $\pm\boldsymbol{G}_0$ generator pair. Rotate one of the icosahedrons (either one will do, but the figure shows the one of the left panel of Fig. 2) into the configuration of Fig 3. Then the vectors of the three suits of the dodecad corresponding to the B-tope into which the A-tope transitions, are all given by a formula such as the one indicated in that figure. There are 1152 symmetries of the dodecad, so there are many valid representations. For example, a cyclic rotation of the diagram by 120° leads to the same dodecad, except with the suits cyclically rotated.

If we consider the generators belonging to the new dodecad that were not part of the original decad, i.e., the generators $\boldsymbol{S}_3^{(i)}$ with $i = 0, 1, 2$, we can verify from the standard tableau of (3.7) that these three vectors do *not* constitute a triad – their sums and differences never result in a null 4-vector. From the symmetries of the dodecads under the linear operations that permute their vertices, there are a total of 48 such 'non-triads' whose loss from the dodecad must therefore result in a transition to a different neighboring A-tope. In the case of the loss of a set of three generator pairs which *are* triads, of which there are 16 instances (one member from each suit), the transition cannot be to another A-tope and must therefore result in a transition to a neighboring B-tope. We are not ultimately interested so much in the transitions between the B-topes themselves, as we really want to further decompose them into smaller 10-simplex fragments first. But we note that, as the line-smoothing weights associated with *any* set of three generator pairs of the dodecad go to zero, a transition occurs at which only nine weights generically remain nonzero, implying that the boundary element at which this occurs is a 9-simplex (in eight dimensions). Thus, the B-tope is bounded by 64 9-simplexes, 48 of them separating the B-tope from an A-tope and 16 of them separating it from another B-tope.

We leave discussion of the ways in which the B-tope can be dissected into more useful pieces for a later section. But we have seen how the very large orders of intrinsic symmetry of the A-tope (240) and B-tope (1152) under vertex-permuting linear operations imply that, in order to find *unique* representations of each object (at least, up to uniform sign reversal of all their generators) we need to break these symmetries drastically. The artificial imposition of a Galois field served that purpose in the cases of the Triad and Hexad algorithms, with each member of those polyads always being of a distinct 'color' and the pattern, or '*spectrum*', of colors in those cases allowed each polyad to be uniquely oriented; the question we must answer before we proceed is whether the same is true in the 4D case where the symmetries that need to be broken are of a spectacularly higher order, and where there are *two* species of the tensor-image polytopes to be dealt with, not just *one*.

In the case of the representative decad of (3.5); if we simply ignore the signs of the vector components there, the resulting binary digits of each column are certainly different. If any other valid decad maps to the Galois field in eactly the same way, then, owing to the form of the transition rule depicted in Fig. 3, the imprint into the set of Galois field components of the corresponding neighboring dodecad of this alternative decad will also correspond to the dodecad neighbor of our original reference decad. The 'colors' of the members of the reference default decad of (3.6) and the 'colors' of the dodecad resulting from the transition depicted in

TABLE 2. Table of the standard tableau indices of the vertices v_k of the generator polytope, arranged by colors in the case where each decad is at a color off-set of 0. The empty slots are denoted by 'X' and the sequences of 'gaps' between these unoccupied g_k are listed in the last column. The horizontal line partitions equivalence classes related to each other by kinship under the squaring automorphism of the associated Galois field.

K	g_0	g_1	g_2	g_3	g_4	g_5	g_6	g_7	g_8	g_9	g_{10}	g_{11}	g_{12}	g_{13}	g_{14}	Gaps
0	X	6	8	X	X	X	X	7	3	9	5	1	0	2	4	3,1,1,1,9
1	X	3	6	9	8	5	X	1	X	0	X	2	X	4	7	6,2,2,2,3
2	X	X	3	0	6	X	9	2	8	X	5	4	X	7	1	1,4,4,3,3
3	X	8	X	X	3	5	0	4	6	X	X	7	9	1	2	2,1,6,1,5
4	X	X	X	8	6	4	X	X	7	3	9	2	1	0	5	1,1,4,1,8
5	X	7	X	3	X	9	8	2	6	1	4	0	X	5	X	2,2,8,2,1
6	X	6	7	1	X	4	3	0	X	X	9	5	8	X	2	4,4,1,4,2
7	X	X	6	X	7	9	1	5	X	8	4	X	3	2	0	1,2,5,3,4
8	9	X	0	5	X	4	X	7	3	X	X	1	8	6	2	3,2,3,1,6
9	9	3	X	X	0	X	5	1	X	8	4	6	X	2	7	1,2,3,4,5
10	X	1	5	9	6	4	2	X	7	8	3	X	0	X	X	4,2,1,1,7
11	X	7	0	X	9	8	X	4	1	X	3	5	X	2	6	3,3,3,3,3
$\overline{\mathcal{L}} \equiv 12{:}27$	X	2	X	6	1	0	4	11	X	8	3	10	9	7	5	2,6,7
$\overline{\mathcal{L}}' \equiv 28{:}43$	X	X	2	8	X	3	6	10	1	9	0	7	4	5	11	1,3,11
$\overline{\mathcal{L}}'' \equiv 44{:}59$	X	2	1	11	0	X	6	7	3	5	X	8	10	4	9	5,5,5

Fig. 3 are the *ordered* sets:

$$\text{Galois colors of } (\boldsymbol{G}_i'|\boldsymbol{H}_i') = (2, 1, 0, 13, 9|3, 8, 12, 7, 14) \tag{3.8a}$$

$$\text{Galois colors of } (\boldsymbol{S}_i^{(0)}|\boldsymbol{S}_i^{(1)}|\boldsymbol{S}_i^{(2)}) = (3, 12, 7, 6|1, 8, 0, 5|9, 13, 14, 11), \tag{3.8b}$$

and the colors that are *missing* from these polyads are:

$$\text{Colors } \textbf{not} \text{ in } (\boldsymbol{G}_i'|\boldsymbol{H}_i') = \{4, 5, 6, 10, 11\} \tag{3.9a}$$

$$\text{Colors } \textbf{not} \text{ in } (\boldsymbol{S}_i^{(0)}|\boldsymbol{S}_i^{(1)}|\boldsymbol{S}_i^{(2)}) = \{2, 4, 10\}. \tag{3.9b}$$

Not only are we encouraged by seeing that the colors present in the neighboring dodecad are all distinct, but we notice that the missing colors corresponds to a triad or, in the terminology of the finite projective geometry, to a 'line' of $PG(3, 2)$. There is nothing about the way we have chosen to map the lattice of generators into this finite projective space that would make this particular 'line' special; on the contrary, we should expect that, if one dodecad has colors that are the complement of those that form a line, then the colors of *all* of the possible dodecads should correspond to the complements of the 35 various lines of $PG(3, 2)$, and this proves to be the case. It is convenient to denote the 15 dodecads with line-complements of the type $\mathcal{L}$ the set, $\overline{\mathcal{L}}$, the 15 with line-complements of type $\mathcal{L}'$ the set, $\overline{\mathcal{L}}'$, and the five that complement lines of the type $\mathcal{L}''$ the set $\overline{\mathcal{L}}''$. We also observe that, for each suit, the $PG(3, 2)$ points that label its four generators all belong to one plane of that finite projective geometry – the other three points of the plane being those of the aforementioned line which complements 12 points of the dodecad. The example (3.8b) of a dodecad happens to be a complement of a member of the family of lines we denoted $\mathcal{L}$ according to (2.1a), but the other families are represented by other corresponding families of dodecads, and the incidence sequences, or spectra, within the cyclic set, $\{0, \ldots, 14\}$, of colors, are the same for each line and uniquely identifies it – a kind of 'fingerprint'. Naturally, we choose to make the sequence associated with each of the three line types $\mathcal{L}$, $\mathcal{L}'$ and $\mathcal{L}''$, identical apart from the necessary color shift modulo-15 (for $\mathcal{L}$, $\mathcal{L}'$) or modulo-5 (for $\mathcal{L}''$). We also exploit the fact that the squaring automorphism interchanges the lines of $\mathcal{L}$ and $\mathcal{L}'$, so we can exploit this additional symmetry when we standardize the labeling of the vertex-pairs of each dodecad.

Given that we have found a helpful correspondence of the dodecads with the line and plane elements of $PG(3, 2)$, we seek a corresponding 'geometrical' interpretation, within $PG(3, 2)$, of the objects we have called the 'decads'. It turns out that the A-tope decad has a subset of ten colors which:

(i) Does not contain any plane of $PG(3, 2)$

(ii) Contains a unique plane each time just one of the missing colors is included.

TABLE 3. Table of the relative Galois field 'colors' g_k of the vertices v_k of each A-tope

K	v_0	v_1	v_2	v_3	v_4	v_5	v_6	v_7	v_8	v_9
0	12	11	13	8	14	10	1	7	2	9
1	9	7	11	1	13	5	2	14	4	3
2	3	14	7	2	11	10	4	13	8	6
3	6	13	14	4	7	5	8	11	1	12
4	13	12	11	9	5	14	4	8	3	10
5	11	9	7	3	10	13	8	1	6	5
6	7	3	14	6	5	11	1	2	12	10
7	14	6	13	12	10	7	2	4	9	5
8	2	11	14	8	5	3	13	7	12	0
9	4	7	13	1	10	6	11	14	9	0
10	12	1	6	10	5	2	4	8	9	3
11	2	8	13	10	7	11	14	1	5	4

TABLE 4. Table of the relative Galois field 'colors' g_k of the vertices v_k of each class of B-tope

K	v_0	v_1	v_2	v_3	v_4	v_5	v_6	v_7	v_8	v_9	v_{10}	v_{11}
$\overline{\mathcal{L}} \equiv 12{:}27$	5	4	1	10	6	14	3	13	9	12	11	7
$\overline{\mathcal{L}}' \equiv 28{:}43$	10	8	2	5	12	13	6	11	3	9	7	14
$\overline{\mathcal{L}}'' \equiv 44{:}59$	4	2	1	8	13	9	6	7	11	14	12	3

When this geometrical specification is adopted and applied to every possible subset of ten colors, we find that the number of possible decad color configurations is 168. This is the number we expect when we remember that each B-tope has 48 neighboring A-topes, and each A-tope has 10 neighboring B-topes, since we have established already that the number of color combinations for the B-topes is 35. ($168 = 48 \times 35/10$). Eleven patterns exist subject to a color off-set in the range 0–14, and one, with a cyclically symmetric pattern to its missing colors (i.e, every third one) exists subject to a color off-set 0–2. These 'incidence patterns' are all tabulated with what we have chosen as the 'default' color rotation, in Table 2, together with those of the dodecads, whose identifiers (labels K), anticipating their future further dissections into smaller pieces, are gathered into bundles of 16 at the bottom of the table. In the last column is listed the cyclic sequence of 'gaps' in the complementary incidence pattern imprinted by the missing colors (these cyclic sequential gaps are invariant to color off-set, and the fact that each is recognizably distinct from the others confirms that each type of decad or dodecad can be both recognized from its colors, and uniquely oriented by means of this table of standardized vertex assignments. An alternative and often more convenient tabulation of the same information is obtained in Tables 3 and 4, where the Galois colors, g_k, are listed for each standardized polyad vertex, v_k, for the A-topes and B-topes.

If we refer back to the example of the decad of (3.8a) we find that it fits the exact pattern in Table 3 at row $K = 4$ except for the colors g_k cyclically shifted by four places. The dodecad it transitions into, i.e., that of (3.8b) can be found, in a slightly permuted form, in the row of the table that corresponds to $K \in \overline{\mathcal{L}}$ with a color shift of two places, and where the permutations are all within each respective suit. The exact arrangements of the decads and dodecads in the table are somewhat arbitrary, and not necessarily the most symmetric taken as a whole, but they do enable us to orient all the polyads in an unambiguous way once these conventions for what we regard to be the 'standard' orientations are agreed upon.

We can verify that, subject to repeats of the now-familiar squaring automorphism, these decads and dodecads stay within various equivalence classes, cycling through with periods of one, two, or four. The dodecads in the sets $\overline{\mathcal{L}}$ and $\overline{\mathcal{L}}'$ form one equivalence class with period-2, leaving those in the set $\overline{\mathcal{L}}''$ in a period-1 class by themselves. The A-tope decads fall into five equivalence classes. The first, of period-4, each have just one of their neighbor B-topes of belonging to the class $\overline{\mathcal{L}}''$, while the second equivalence class, also of period-4, all have two such neighbors. There is a class of period-2 that also have two neighbors in $\overline{\mathcal{L}}''$. One of the two period-1 classes of the decads has 15 color types, and the other period-1 class has a color spectrum with the five-fold periodicity that implies that it can possess only three distinguishable color sub-types. In the cases of classes of period-4, the standard presentation in each member of the class can be chosen to make it a straightforward squaring automorphism of the member that preceeds it in a cyclic sense. But in the cases of equivalence classes of period-2, we can standardize the arrangement of generators in the first member, and arrange to make the second follow directly from it by the squaring automorphism, but then the first only follows from the second when this automorphism is combined with a rotation, or permutation of the vertices of the A-tope. Likewise, for the classes with only one member each, they map into themselves under this automorphism, but only with a rotation (which itself forms a cyclic group of period-4). The tables respect these subdivisions into equivalence classses, which involve the identifying indices, K, for the A-topes defining the cycles $(0:3)$, $(4:7)$, $(8:9)$, (10) and (11) (this last being the one with only three color variants, owing to the five-fold periodicity of its color spectrum).

Next we deal with the problem of constructing true decads – preimages within the space of generator-pairs, of 10-simplex partitions of the B-topes.

4. partitioning the B-topes into 10-simplexes

Recall that, in the case of the B-tope, the + and - generators that correspond to the 12 vertices have a convex hull which, under an isotropizing linear distortion, corresponds to the regular 24-cell polytope in 4D. Their vertices then fall naturally into three sets or 'suits' whose eight generators are vertices of an orthoplex. That is, four + and − copies of orthogonal vectors corresponding to all the $\boldsymbol{S}^{(0)}$, or all the $\boldsymbol{S}^{(1)}$, or all the $\boldsymbol{S}^{(2)}$ of the dodecads. We can permute the four independent generators of suit $S^{(0)}$ (24 symmetries) and we can switch their signs (×16 symmetries), and we can further replace our suit $\boldsymbol{S}^{(0)}$ ('suit-0') by either the suit-1 or the suit-2 (×3 further symmetries), using the linearity relationships of DODEC0 of (3.7) to regenerate the remaining generators – that's 1152 symmetries in all.

Restricting to symmetries that preserve the three suits reduces the number again by a factor 1/6, resulting in 192 suit-preserving symmetries. Owing to the mutual orthogonality of the four independent generators in each suit in the isotropizing frame, the aspect centroids of the three suits coincide, being therefore the aspect centroid of the whole B-tope. We call this central aspect point the '*hub*'; it is useful for anchoring the further dissections of the B-tope into true simplexes. As previously noted, if we remove one member from each suit and take the convex hull of the resulting 9-point object in aspect space, we obtain a 9-simplex in an affine space of eight dimensions that forms one boundary flat of the B-tope; all boundary flats are of this form. Since there are $4 \times 4 \times 4 = 64$ different ways of downsizing the suits in this way, our B-tope is 64-sided and can be dissected into true 10-simplexes by augmenting each boundary 9-simplex, one at a time, with the hub and taking the convex hull. Note, however, that the hub does **not** possess a preimage in the form of any single generator, so the 64 10-simplexes obtained in this way do not immediately solve the problem of decomposing the preimage of this portion of the aspect space into equivalent decads.

Also, we note that these 64 10-simplexes are not all congruent. When we pick one suit-0 vector, one suit-1 vector, and one suit-2 vector for exclusion, two cases can occur:

(i) the excluded vectors can form a linearly **dependent** '*triad*', which can occur in 16 ways;

(ii) they can form a linearly **independent** '*non-triad*', which can occur in 48 ways.

The combinations of three generator vectors, each from a different suit, that form dependent triads (and thus map to respective 'lines' of $PG(3, 2)$) form 16 4×3 arrays, S_a, indexed, $a \in \{0 : 15\}$,

$$\mathsf{S}_a = \left[\ \boldsymbol{S}^{(0)}_{i_a} \quad \boldsymbol{S}^{(1)}_{j_a} \quad \boldsymbol{S}^{(2)}_{k_a}\ \right], \qquad i_a, j_a, k_a \in [0 : 3] \tag{4.1}$$

where the column vectors are taken from the tableau (3.7). To each S_a, an associated 'sign'-vector, $\boldsymbol{\sigma}_a^{\mathsf{T}} = (\sigma_a^{(0)}, \sigma_a^{(1)}, \sigma_a^{(2)})$ with $\sigma_a^{(m)} = \pm 1$, serves to define the triad conditions in matrix notation:

$$\mathsf{S}_a {\cdot} \boldsymbol{\sigma}_a = \mathbf{0}, \tag{4.2}$$

where the 16 index-triples, $\{i_a, j_a, k_a\}$, and sign-vectors, $\boldsymbol{\sigma}_a$, can be formally defined:

$$i_a \;=\; a \pmod 4 \tag{4.3a}$$

$$j_a \;=\; \lfloor(a/4) \tag{4.3b}$$

$$k_a \;=\; \left\{ \begin{array}{rcl} 3 & : & i_a + j_a = 3 \\ |i_a - j_a| & : & \text{otherwise} \end{array} \right. , \tag{4.3c}$$

and, with the aid of the usual Kronecker delta:

$$\sigma_a^{(0)} \;=\; 2 - \delta_{i_a, j_a} \tag{4.4a}$$

$$\sigma_a^{(1)} = 2 - \delta_{i_a,0} \tag{4.4b}$$
$$\sigma_a^{(2)} = 2 - \delta_{0,j_a} \tag{4.4c}$$

These 16 triads of the dodecad in its standard form are listed in Table 5

TABLE 5. Triads of the standardized dodecad

	$j_a = 0$			$j_a = 1$			$j_a = 2$			$j_a = 3$		
i_a	a	$\boldsymbol{\sigma}_a$	k_a	a	$\boldsymbol{\sigma}_a$	k_a	a	$\boldsymbol{\sigma}_a$	k_a	a	$\boldsymbol{\sigma}_a$	k_a
0	0	$---$	0	4	$+-+$	1	8	$+-+$	2	12	$+-+$	3
1	1	$++-$	1	5	$-++$	0	9	$+++$	3	13	$+++$	2
2	2	$++-$	2	6	$+++$	3	10	$-++$	0	14	$+++$	1
3	3	$++-$	3	7	$+++$	2	11	$+++$	1	15	$-++$	0

If we ignore the signs and consider only the indices themselves to form integer 3-vectors, these instances collectively trace out the corners and joining edges of a tetrahedron in the cube, $[0:3] \times [0:3] \times [0:3]$ of the index lattice. We shall call the 48 sub-simplexes whose non-hub nonets are complements of the non-triads the '*C-topes*' of this B-tope. We shall call the 16 subsimplexes whose non-hub nonets are complements of triads the '*D-topes*' of this B-tope.

To recapitulate, a B-tope is the union of 48 C-topes and 16 D-topes. This dissection enables us to navigate in aspect space from one simplex to another, almost as we do in the 2D triad or the 3D hexad algorithm, except now our simplexes come in three varieties and we must know how they make contact with one another. The connectivity is summarized as follows

(i) Each A-tope meets the C-topes of 10 different neighboring parent B-topes on each of the A-tope's ten sides;

(ii) Each C-tope meets an *exterior* A-tope of the side opposite the hub (being the converse relationship to (i);

(iii) Each C-tope meets another *interior* (same B-tope) C-tope on six of its other sides;

(iv) Each C-tope meets interior D-topes at its remaining three sides.

(v) Each D-tope meets an exterior D-tope (from a neighboring B-tope) across the side opposite the hub;

(vi) Each D-tope meets only interior C-topes on its remaining nine sides.

We might inquire: how do we know whether the C-tope's interior neighbor is a C-tope or a D-tope? First, some more terminology. We call the three B-tope vertices that do NOT belong to a contained C-tope the '*non-vertices* of that C-tope, and likewise for a contained D-tope. To answer our question, when the opposite vertex of the original C-tope forms a non-triad with the two non-vertices of the other suits, that side of the C-tope abuts an interior C-tope; if on the contrary, the opposing vertex plus the two non-vertices of the other suits form a triad, then contact is made with an interior D-tope.

While this description of the geometry of the tensor-images of generators of the 4D lattice helps us to navigate through the aspect space tiled by the various A-tope, C-tope and D-tope 10-simplexes, we are not yet able to use these structures to define decads of generators (except in the case of the A-topes) because the hub points shared by the C- and D-topes of a B-tope have no single preimage in the form of a lattice generator. An early form of the algorithm exploited the fact that the preimages of all twelve of the vertices of the parent B-tope, which had the hub as its centroid, could be attributed an equal additional amount of smoothing 'weight' in the appropriate proportion to the aspect tensor projection onto the 10-vector defining the hub. This was in order to partially mimic a true decad algorithm. However, this required that, at most points of the geographical filtering lattice, a positive amount of line smoothing was required to be applied along no less than twelve distinct line directions. In order to achieve a more satisfactory algorithm involving *only* true decads of generators at each lattice point, we need to find some way to dissect the 12-point polytopes of the aspect space into 10-simplexes whose vertices all belong to the original set of twelve. Moreover, for continuity of the smoothing operations on the 4D lattice, it is important that a way is found to ensure that the dissection is carried out in exactly the *same* way each time this particular 12-point polytope is encountered.

We find that the hub point is the centroid not just of the set of twelve vertices of the parent B-tope, but of each suit of four vertices of that B-tope separately. This means that, in principle, the interior aspect vectors of either a C-tope or a D-tope can be obtained by a barycentric weighting of their nonet of B-tope-boundary generators plus one set of four equally-weighted suit members from a **single** chosen suit, making the total number of involved generators 10, exactly as we would wish. Since any suit can be chosen for this honor there are three ways this can be done for each C-tope or D-tope. The 10 involved generators imply a new 10-simplex in aspect space of the type we shall refer to henceforth as an 'E-tope'. Note that each E-tope is distinguished by its characteristic suit (used to imply the hub weighting) and, to each suit there are associated 16 different and non-overlapping E-topes whose union forms the whole of the parent B-tope. Each E-tope is thus the union of 3 C-topes and one D-tope. Referring back to Table 5 implicitly defining the symbolic $[0:3]\times[0:3]\times[0:3]$ lattice of complement-indices, where each of the 64 points could be identified with either a C-tope or a D-tope, we can now identify all the E-topes of a given suit with the 16 parallel lines (aligned with that suit coordinate) in this little symbolic lattice, and verify that each contains one (and only one) of the designated D-tope images.

In order to dissect each B-tope into constituent disjoint E-topes in a uniquely defined way, we rotate it in such a way that the Galois colors of its ordered sequence of 12 vertices exactly matches (within a uniform cyclic color shift) one of the patterns implied by one of the last three rows of Table 2. Apart from the color off-set, the four generators of suit-0 are to found at the (relative) colors of this table at which we find the quartet of vertex indices, $\{0,1,2,3\}$, those of suit-1 where we find $\{4,5,6,7\}$ and those of suit-2 where we find vertex labels, $\{8,9,10,11\}$. Thus, the projection into $GF(16)$ also largely takes care of sorting out the geometry of the generators relative to one another. This enables us to *always* choose to decompose the B-tope dodecad into its 16 component E-topes with the now identified suit-0 as the 'special' one, as discussed above. Recall that each component E-tope is obtained from the parent B-tope by omitting one B-tope vertex from suit-1 and one vertex from suit-2.

It is convenient, for the purposes of efficient tabulation, if we can re-label the B-tope vertices in each case such that the omitted pair are the *last* members of the respective suits 1 and 2 after this re-labeling. It is also very convenient if all 12 of the generators of the B-tope have their relative orientations, i.e., their signs, arranged in such a way that, if 'DODEC' denotes the matrix of 12 column 4-vectors arranged in three blocks of four, then this matrix is derived from the first four of them, which we denote 'BASIS', by the matrix-multiplication rule,

$$\mathrm{DODEC} = (\mathrm{BASIS}\times\mathrm{DODEC0})/2 \tag{4.5}$$

TABLE 6. Table of the standardized Galois field 'colors' g_k of the vertices v_k of each E-tope of the B-sets of type $\overline{\mathcal{L}}$. 'K' is the identifier of each particular E-tope decad type.

K	v_0	v_1	v_2	v_3	v_4	v_5	v_6	v_7	v_8	v_9
12	10	1	4	5	14	6	13	11	7	9
13	4	5	10	1	13	3	14	11	7	9
14	5	4	1	10	3	13	6	11	7	9
15	1	10	5	4	6	14	3	11	7	9
16	5	4	1	10	14	6	13	12	9	7
17	1	10	5	4	13	3	14	12	9	7
18	10	1	4	5	3	13	6	12	9	7
19	4	5	10	1	6	14	3	12	9	7
20	1	10	5	4	14	6	13	7	11	12
21	5	4	1	10	13	3	14	7	11	12
22	4	5	10	1	3	13	6	7	11	12
23	10	1	4	5	6	14	3	7	11	12
24	4	5	10	1	14	6	13	9	12	11
25	10	1	4	5	13	3	14	9	12	11
26	1	10	5	4	3	13	6	9	12	11
27	5	4	1	10	6	14	3	9	12	11

where 'DODEC0' is the matrix exactly as defined in (3.7). This rule obviously exploits the fact that the first four columns, making up suit-0, of DODEC0, are just twice the identity matrix.

If we consider the group of operations that combine the even permutations of the columns of suit-0 indicated by the '*Klein 4-group*' representation:

$$\begin{aligned} V_0 &= (0,1,2,3) \\ V_1 &= (1,0,3,2) \\ V_2 &= (2,3,0,1) \\ V_3 &= (3,2,1,0) \end{aligned} \tag{4.6}$$

combined with a possible switching of the signs of the permuted columns, we find that the vectors of suit-1 are permuted amongst themselves and the vectors of suit-2 are permuted amongst themselves (possibly with sign-switches) in such a way that it is always possible to find a way to place the generators designated for omission at the desired locations, nominally new columns 7 and 11. We can now give to each E-tope's true decad, an identifier that distinguishes it amongst the 16 belonging to the same B-tope, and list the colors, relative to its off-set, of the newly labeled 10 vertices, where vertices 0–3 are the newly ordered vertices still of suit-0, vertices 4–6 are the three remaining of suit-1, and vertices 7–9 are those remaining of suit-2.

With the convention established, we can derive the full representative set of generators of an E-tope from the same basis, suitably permuted, by applying to the same basis of first-four

TABLE 7. Table of the relative Galois field 'colors' g_k of the vertices v_k of each E-tope of the B-sets of type $\overline{\mathcal{L}}'$. 'K' is defined as in Table 6.

K	v_0	v_1	v_2	v_3	v_4	v_5	v_6	v_7	v_8	v_9
28	5	2	8	10	13	12	11	7	14	3
29	8	10	5	2	11	6	13	7	14	3
30	10	8	2	5	6	11	12	7	14	3
31	2	5	10	8	12	13	6	7	14	3
32	10	8	2	5	13	12	11	9	3	14
33	2	5	10	8	11	6	13	9	3	14
34	5	2	8	10	6	11	12	9	3	14
35	8	10	5	2	12	13	6	9	3	14
36	2	5	10	8	13	12	11	14	7	9
37	10	8	2	5	11	6	13	14	7	9
38	8	10	5	2	6	11	12	14	7	9
39	5	2	8	10	12	13	6	14	7	9
40	8	10	5	2	13	12	11	3	9	7
41	5	2	8	10	11	6	13	3	9	7
42	2	5	10	8	6	11	12	3	9	7
43	10	8	2	5	12	13	6	3	9	7

4-vectors, a right-multiplication by the 4 × 12 matrix:

$$\mathrm{DODEC0T} = \left[\begin{array}{cccc|ccc|ccc} 2 & 0 & 0 & 0 & -1 & 1 & 1 & -1 & -1 & -1 \\ 0 & 2 & 0 & 0 & -1 & 1 & -1 & 1 & 1 & -1 \\ 0 & 0 & 2 & 0 & -1 & -1 & 1 & 1 & -1 & 1 \\ 0 & 0 & 0 & 2 & -1 & -1 & -1 & 1 & -1 & -1 \end{array}\right], \tag{4.7}$$

and dividing the result by two.

We systematically decompose the B-tope whose color-complement is the line type $\mathcal{L}$, into the 16 E-topes identified by the index $K \in \{12 : 27\}$. Similarly, the B-tope with complement $\mathcal{L}'$ becomes the set with $K \in \{28 : 43\}$. The E-topes from the B-tope the color-complement $\mathcal{L}''$ become those with $K \in \{44 : 59\}$. Now that we have fully decomposed the aspect space uniquely into 60 K-types of decads, we can list the off-set-0 color versions of each of these types in a way that remains consistent with Table 2. We have already seen that Table 3 lists the relative colors of the vertices of the A-topes; Table 6 lists the same for the the E-topes of complement-$\mathcal{L}$ and Table 7 the corresponding data for the complement of the $\mathcal{L}'$. Table 8 tabulates the relative colors of the vertices of the E-topes whose color spectra exhibit the three-fold symmetry, i.e., complement-$\mathcal{L}''$.

When we apply the squaring automorphism, we find that each K-type is transformed into a K-type of the same equivalence class, but not necessarily with the same K. A table of these K-type images under the application of this automorphism is given (with some obvious redundancy) by Table 9.

With the global status of the A-tope and E-tope decad tilings now defined, we can compute the remaining needed combinatorial attributes. For example, opposite to each vertex, v_i of the

TABLE 8. Table of the relative Galois field ‘colors’ g_k of the vertices v_k of each E-tope of the B-sets of type $\overline{\mathcal{L}}''$. ‘K’ is defined as in Table 6.

K	v_0	v_1	v_2	v_3	v_4	v_5	v_6	v_7	v_8	v_9
44	1	8	4	2	9	13	7	3	12	14
45	2	4	8	1	6	7	13	3	12	14
46	4	2	1	8	7	6	9	3	12	14
47	8	1	2	4	13	9	6	3	12	14
48	4	2	1	8	9	13	7	14	11	3
49	8	1	2	4	6	7	13	14	11	3
50	1	8	4	2	7	6	9	14	11	3
51	2	4	8	1	13	9	6	14	11	3
52	8	1	2	4	9	13	7	12	3	11
53	4	2	1	8	6	7	13	12	3	11
54	2	4	8	1	7	6	9	12	3	11
55	1	8	4	2	13	9	6	12	3	11
56	2	4	8	1	9	13	7	11	14	12
57	1	8	4	2	6	7	13	11	14	12
58	8	1	2	4	7	6	9	11	14	12
59	4	2	1	8	13	9	6	11	14	12

TABLE 9. Cycles of the decad type K_n indices n induced by the squaring automorphism of $GF(16)$.

0	1	2	3	12	28			44	51	53	58
1	2	3	0	13	29	20	36	45	59	52	50
2	3	0	1	14	30	16	32	46	47	55	54
3	0	1	2	15	31	24	40	47	55	54	46
				16	32	14	30	48	49	57	56
4	5	6	7	17	33	22	38	49	57	56	48
5	6	7	4	18	34			50	45	59	52
6	7	4	5	19	35	26	42	51	53	58	44
7	4	5	6	20	36	13	29	52	50	45	59
				21	37			53	58	44	51
8	9			22	38	17	33	54	46	47	55
9	8			23	39	25	41	55	54	46	47
				24	40	15	31	56	48	49	57
10				25	41	23	39	57	56	48	49
				26	42	19	35	58	44	51	53
11				27	43			59	52	50	45

A-topes and E-topes, we would like to know what K type of neighbor is found there and with what relative color. This information is provided for the A-topes in the tables 10, 11, and 12. Note that, for a neighbor with a K-type in the range 44–59, corresponding to the complement of lines $\mathcal{L}''$ of $PG(3, 2)$, there are three choices with relative color increments differing by 5 or 10. This is owing to the fact that these neighbors must have their final decad color off-set assignments (relative to the entries of Table 8) restricted to the range $[0:4]$ because of their

3-fold symmetries.

For A-topes in the equivalence class with $K \in \{0:3\}$, listed in Table 10, the neighbor opposite each vertex, v_5, is of the $\mathcal{L}''$-complement type (indices $K \in \{44:59\}$) so there are three listed possibilities for the neighbor K index and relative color, with the choice being, as we have seen, the one that keeps the absolute color off-set of this neighbor within its valid range $[0:4]$ relative to the standardarized (zero off-set) of Table 8.

For the A-topes in the equivalence class with $K \in \{4:7\}$, listed in the left-hand section of Table 11, there are now two vertices, v_1 and v_2, opposite to which the neighbors belong to the $\mathcal{L}''$-complement set where, again, three possibilities need to be tabulated. Apart from this minor complication, each successive column, here and in Table 10, is the result of applying the squaring automorphism to the entries in the preceding column in accordance with the cycling of the K labels set out in Table 9, so the symmetries of $GF(16)$ are providing some redundancy to our tabulations. The right-hand section of Table 11 provides the same information for the equivalence class consisting of the pair, $K \in \{8, 9\}$. And separately, Table 12 provides the data for the single-K classes, $K = \{10\}$ and $K = \{11\}$. In the cases of the equivalence classes $\{K_8, K_9\}$, $\{K_{10}\}$, $\{K_{11}\}$, we indicate, in the respective appended columns, how the squaring automorphism permutes the vertices into the new vertex labels (i.e., 'rotates' the decad orientation) at the point where the cycle begins again. These symmetries have no intrinsic significance beyond the fact that thay can potentially be exploited in the initialization of these tables in the software algorithm from a more compact core of the essential data that implicitly encodes them.

TABLE 10. For decad types $K \in \{0:3\}$, and vertex v_k, the neighbor type K_k and its color increment(s), modulo-15, at the position opposite to vertex v_k.

v_k	$K=0$		$K=1$		$K=2$		$K=3$	
v_0	18	4	34	8	18	1	34	2
v_1	12	3	28	6	12	12	28	9
v_2	25	13	41	11	23	7	39	14
v_3	43	4	27	8	43	1	27	2
v_4	32	14	14	13	30	11	16	7
v_5	56	0	48	0	49	0	57	0
	54	5	46	10	47	5	55	10
	45	10	59	5	52	10	50	5
v_6	36	0	13	0	29	0	20	0
v_7	37	3	21	6	37	12	21	9
v_8	38	2	17	4	33	8	22	1
v_9	42	5	19	10	35	5	26	10

Tables of neighbor K-types and relative color off-sets for the E-topes are given in a slightly different format. The K-type data for the related set of 16 E-topes belonging to a same B-tope $\in \overline{\mathcal{L}}$ are given in Table 13. Again, the options are provided in the cases where the final neighbor color assignment is restricted due to either three-fold or five-fold symmetry of the color spectrum of the associated B-tope or the A-tope. It is only from $K = 18$ that the A-tope of type $K = 11$ is encountered, where the deacd's color is always only 0, 1 or 2. Also, it is only

TABLE 11. For decad types $K \in \{4:9\}$, and vertex v_k, the neighbor type K_k and its color increment(s), modulo-15, at the position opposite to vertex v_k.

v_k	$K=4$		$K=5$		$K=6$		$K=7$		$K=8$		$K=9$		v'_k of K'_8
v_0	20	13	36	11	13	7	29	14	26	2	42	4	$\to v'_3$
v_1	54	2	46	4	47	8	55	1	57	1	56	2	$\to v'_2$
	53	7	58	14	44	13	51	11	58	6	44	12	
	57	12	56	9	48	3	49	6	54	11	46	7	
v_2	52	1	50	2	45	4	59	8	48	4	49	8	$\to v'_1$
	45	6	59	12	52	9	50	3	51	9	53	3	
	44	11	51	7	53	14	58	13	47	14	55	13	
v_3	22	7	38	14	17	13	33	11	19	8	35	1	$\to v'_0$
v_4	40	1	15	2	31	4	24	8	43	5	27	10	$\to v'_4$
v_5	24	14	40	13	15	11	31	7	20	1	36	2	$\to v'_8$
v_6	32	0	14	0	30	0	16	0	33	9	22	3	$\to v'_7$
v_7	25	0	41	0	23	0	39	0	38	6	17	12	$\to v'_6$
v_8	42	2	19	4	35	8	26	1	13	4	29	8	$\to v'_5$
v_9	31	6	24	12	40	9	15	3	28	0	12	0	$\to v'_9$

TABLE 12. For decad types $K = 10$ and $K = 11$, and vertex v_k, the neighbor type K_k and its color increment(s), modulo-15, at the position opposite to vertex v_k.

v_k	$K=10$		v'_k of K's	$K=11$		v'_k of K's
v_0	39	11	$\to v'_8$	34	2	$\to v'_9$
v_1	14	14	$\to v'_5$	34	8	$\to v'_7$
v_2	23	13	$\to v'_0$	18	13	$\to v'_5$
v_3	37	10	$\to v'_4$	18	10	$\to v'_8$
v_4	21	5	$\to v'_3$	18	7	$\to v'_6$
v_5	30	13	$\to v'_6$	34	11	$\to v'_4$
v_6	16	11	$\to v'_7$	34	14	$\to v'_2$
v_7	32	7	$\to v'_1$	18	1	$\to v'_0$
v_8	25	7	$\to v'_9$	34	5	$\to v'_3$
v_9	41	14	$\to v'_2$	18	4	$\to v'_1$

opposite the vertex v_0 of all these E-tope K-types that we encounter neighbors of a different B-tope with $K \in \overline{\mathcal{L}}''$, where the three-fold color symmetry occurs. The appended extra row of this table indicates which K is the image under the application of the squaring automorphism (which is trivial in this particular table, since we simply add 16). The relative colors for the 'interior' neighbors (same parent B-tope), opposite vertices v_k with $k > 3$ are always zero, and are therefore omitted. In Table 14, we present the corresponding data for $K \in \overline{\mathcal{L}}'$, and notice that it is from only $K = 34$, opposite v_3 again, that we need to accommodate the special symmetry of the $K = 11$ neighbor. The appended right columns indicate how the vertex labels become permuted by the squaring automorphism when we cycle back to the Ks in the previous range, $12 - 27$, (i.e., the Ks in $\overline{\mathcal{L}}$, and the appended bottom rows are no longer trivial, since the squaring automorphism now permutes *both* rows and columns as we cycle back. Finally, the

TABLE 13. For decad types $K \in \overline{\mathcal{L}}$ and vertex v_k, the neighbor type K_k and its color increment(s), modulo-15, at the position opposite to vertex v_k.

v_k	$K=12$		$K=13$		$K=14$		$K=15$		$K=16$		$K=17$		$K=18$		$K=19$	
v_0	27	10	19	4	16	12	39	12	14	3	55 45 48	1 6 11	34	10	13	11
v_1	0	12	8	11	5	0	5	13	10	4	6	2	0	11	1	5
v_2	2	3	1	0	10	1	7	12	7	0	9	3	2	14	5	11
v_3	9	0	6	8	1	2	6	4	3	8	1	11	11	$2+3t$	8	7
v_4	14		15		12		13		18		19		16		17	
v_5	13		12		15		14		17		16		19		18	
v_6	15		14		13		12		19		18		17		16	
v_7	16		17		18		19		12		13		14		15	
v_8	24		25		26		27		20		21		22		23	
v_9	20		21		22		23		24		25		26		27	
K'	$\hookrightarrow 28$		$\hookrightarrow 29$		$\hookrightarrow 30$		$\hookrightarrow 31$		$\hookrightarrow 32$		$\hookrightarrow 33$		$\hookrightarrow 34$		$\hookrightarrow 35$	

v_k	$K=20$		$K=21$		$K=22$		$K=23$		$K=24$		$K=25$		$K=26$		$K=27$	
v_0	26	1	37	5	46 52 47	4 9 14	40	9	41	3	31	6	20	14	12	5
v_1	3	0	1	9	9	12	10	2	5	3	4	0	7	14	1	7
v_2	8	14	3	6	4	8	6	0	7	7	10	8	3	5	3	13
v_3	4	2	10	10	3	14	2	8	4	1	0	2	8	13	9	5
v_4	22		23		20		21		26		27		24		25	
v_5	21		20		23		22		25		24		27		26	
v_6	23		22		21		20		27		26		25		24	
v_7	24		25		26		27		20		21		22		23	
v_8	16		17		18		19		12		13		14		15	
v_9	12		13		14		15		16		17		18		19	
K'	$\hookrightarrow 36$		$\hookrightarrow 37$		$\hookrightarrow 38$		$\hookrightarrow 39$		$\hookrightarrow 40$		$\hookrightarrow 41$		$\hookrightarrow 42$		$\hookrightarrow 43$	

Table 15 provides the data for the E-topes in $\overline{\mathcal{L}}''$ whose parent B-tope's color spectrum exhibits the three-fold symmetry. The options in the v_0-row are only of two choices in the particular cases $K = 44, 51, 53, 58$ where the exterior neighbor is another $\mathcal{L}''$-complement E-tope.

To make the algorithm that resolves each given aspect tensor in its proper decad efficient, additional tables must be set up to define how a transition from one decad to its neighbor shuffles the colors of the nine generators that remain in common to the new decad's vertices, as well as recording both the color of the old decad lost and the color of the new decad gained, in *their* proper places in the vertex list. This is most conveniently done by tabulations of permutations amongst the ten vertex labels. Also tabulated for each possible transition are the 4×4 matrices that transform the old basis set (first four of the 4-vectors of the A-tope or E-tope) to the new basis set. By performing the transformation this way at all the intermediate steps of the iterative solution procedure, it is not actually necessary to recompute at each step the full set of each decad's 4-vectors. However, we must have a mechanism to tell the algorithm

TABLE 14. For decad types $K \in \overline{\mathcal{L}}'$ and vertex v_k, the neighbor type K_k and its color increment(s), modulo-15, at the position opposite to vertex v_k.

v_k	$K = 28$		$K = 29$		$K = 30$		$K = 31$		$K = 32$		$K = 33$		$K = 34$		$K = 35$		v'_k of $K' \in \overline{\mathcal{L}}$
v_0	43	5	35	8	32	9	25	9	30	6	54 59 49	2 12 7	18	5	29	7	$\to v'_0$
v_1	1	9	9	7	6	0	6	11	10	8	7	4	1	7	2	10	$\to v'_2$
v_2	3	6	2	0	10	2	4	9	4	0	8	6	3	13	6	7	$\to v'_1$
v_3	8	0	7	1	2	4	7	8	0	1	2	7	11	$4+3t$	9	14	$\to v'_3$
v_4	30		31		28		29		34		35		32		33		$\to v'_7$
v_5	29		28		31		30		33		32		35		34		$\to v'_9$
v_6	31		30		29		28		35		34		33		32		$\to v'_8$
v_7	32		33		34		35		28		29		30		31		$\to v'_4$
v_8	40		41		42		43		36		37		38		39		$\to v'_6$
v_9	36		37		38		39		40		41		42		43		$\to v'_5$
K'	$\hookrightarrow 12$		$\hookrightarrow 20$		$\hookrightarrow 16$		$\hookrightarrow 24$		$\hookrightarrow 14$		$\hookrightarrow 22$		$\hookrightarrow 18$		$\hookrightarrow 26$		

v_k	K_{36}		$K = 37$		K_{38}		$K = 39$		K_{40}		$K = 41$		K_{42}		$K = 43$		v'_k of $K' \in \overline{\mathcal{L}}$
v_0	42	2	21	10	47 50 56	8 3 13	15	3	23	6	24	12	36	13	28	10	$\to v'_0$
v_1	0	0	2	3	8	9	10	4	6	6	5	0	4	13	2	14	$\to v'_2$
v_2	9	13	0	12	5	1	7	0	4	14	10	1	0	10	0	11	$\to v'_1$
v_3	5	4	10	5	0	13	3	1	5	2	1	4	9	11	8	10	$\to v'_3$
v_4	38		39		36		37		42		43		40		41		$\to v'_7$
v_5	37		36		39		38		41		40		43		42		$\to v'_9$
v_6	39		38		37		36		43		42		41		40		$\to v'_8$
v_7	40		41		42		43		36		37		38		39		$\to v'_4$
v_8	32		33		34		35		28		29		30		31		$\to v'_6$
v_9	28		29		30		31		32		33		34		35		$\to v'_5$
K'	$\hookrightarrow 13$		$\hookrightarrow 21$		$\hookrightarrow 17$		$\hookrightarrow 25$		$\hookrightarrow 15$		$\hookrightarrow 23$		$\hookrightarrow 19$		$\hookrightarrow 27$		

whether the present decad is the solution, or, if not, which neighbor it should transition to. In all the polyad algorithms, this is decided by examining the set of ten 'weights', W_i, associated with each of the generators g_i of the decad. If all the weights are non-negative (in practice, to avoid a numerical stalemate, the actual criterion is whether all the weights are greater than a very small negative threshold) then we deem the solution to be the present decad; if not, we locate the most negative of these projected aspect weights, and transition to the decad neighbor opposite to this indicated vertex of the tensor image 10-simple (the A-tope or E-tope) of the present decad. In making the transition, all the projected aspect weights change, of course, but they change in a very simple way since the linear system they solve involves a matrix L (the matrix with columns made of the tensor images of each of the generator self-exterior products), so only one column of this matrix changes when the transition is made. The well-known Sherman-Morrison-Woodbury formula (e.g., Press et al., 1989) applied to this case informs us that the inverse of the matrix changes by a rank-1 update. In the context of the

TABLE 15. For decad types $K \in \overline{\mathcal{L}}''$ and vertex v_k, the neighbor type K_k and its color increment(s), modulo-15, at the position opposite to vertex v_k.

v_k	$K = 44$		$K = 45$		$K = 46$		$K = 47$		$K = 48$		$K = 49$		$K = 50$		$K = 51$		v_k'
v_0	53	1	17	9	22	11	38	7	17	4	33	8	38	12	58	2	$\rightarrow v_0'$
		11														12	
v_1	9	3	6	11	1	5	6	7	8	11	2	0	7	12	7	4	$\rightarrow v_3'$
v_2	4	4	0	5	9	8	8	1	6	12	7	9	3	10	5	8	$\rightarrow v_2'$
v_3	6	2	4	9	5	11	2	10	1	0	9	7	5	13	8	6	$\rightarrow v_1'$
v_4	45		44		47		46		49		48		51		50		$\rightarrow v_9'$
v_5	46		47		44		45		50		51		48		49		$\rightarrow v_8'$
v_6	47		46		45		44		51		50		49		48		$\rightarrow v_7'$
v_7	56		57		58		59		52		53		54		55		$\rightarrow v_6'$
v_8	48		49		50		51		44		45		46		47		$\rightarrow v_5'$
v_9	52		53		54		55		56		57		58		59		$\rightarrow v_4'$
K'	$\hookrightarrow 51$		$\hookrightarrow 59$		$\hookrightarrow 47$		$\hookrightarrow 55$		$\hookrightarrow 49$		$\hookrightarrow 57$		$\hookrightarrow 45$		$\hookrightarrow 53$		

v_k	$K = 52$		$K = 53$		$K = 54$		$K = 55$		$K = 56$		$K = 57$		$K = 58$		$K = 59$		v_k'
v_0	22	6	44	4	33	13	17	14	38	2	22	1	51	3	33	3	$\rightarrow v_0'$
				14										13			
v_1	4	14	9	12	4	13	3	5	0	0	8	14	5	1	5	3	$\rightarrow v_3'$
v_2	2	5	6	1	8	4	9	2	5	6	4	3	7	2	1	10	$\rightarrow v_2'$
v_3	6	6	4	8	0	10	7	14	9	13	3	0	8	9	7	7	$\rightarrow v_1'$
v_4	53		52		55		54		57		56		59		58		$\rightarrow v_9'$
v_5	54		55		52		53		58		59		56		57		$\rightarrow v_8'$
v_6	55		54		53		52		59		58		57		56		$\rightarrow v_7'$
v_7	48		49		50		51		44		45		46		47		$\rightarrow v_6'$
v_8	56		57		58		59		52		53		54		55		$\rightarrow v_5'$
v_9	44		45		46		47		48		49		50		51		$\rightarrow v_4'$
K'	$\hookrightarrow 50$		$\hookrightarrow 58$		$\hookrightarrow 46$		$\hookrightarrow 54$		$\hookrightarrow 48$		$\hookrightarrow 56$		$\hookrightarrow 44$		$\hookrightarrow 52$		

solution of the linear system solving for the projected weights, this means that these weights change in a predictable pattern of proportions for each possible transition, and in proportion to the magnitude of the 'most negative' weight attached to the column of the matrix undergoing the change, since this corresponds to the generator that is replaced. It is significant that the determinant of the matrix formed by the ten aspect vectors of each simplex of this algorithm is ± 1; as a consequence, the weight attached to the new 'gained' vertex of the recruited 10-simplex in the transition is positive and exactly of the same magnitude as the negative weight of the 'lost' vertex of the retired 10-simplex. The pattern of all the other these proportions of weight changes relative to the triggering negative weight, which are all integers (of both signs) are precomputed for each type of transitions, and combined with the tabulated permutations for these transitions so that the new vector of weights, W_i', is efficiently computed from the old weights W_i, bypassing the explicit solution of the ten-dimensional linear inversion problem each iteration. The iterative algorithm can always be initiated from the default decad first guess given by (3.6), and the precalculated inverse, $\boldsymbol{L}^{-1}$, of the system matrix for this special starting case can be used to generate the initial weight vector, $\boldsymbol{W}$, by the simple linear projection from the aspect tensor's 10-vector representation, $\boldsymbol{A}$:

$$\boldsymbol{W} = \boldsymbol{L}^{-1}\boldsymbol{A}. \tag{4.8}$$

These additional tables containing the vertex-index permutations, the rank-1 update profile vectors, and the basis transformation matrices for each possible transition, are too voluminous to be given here.

At the termination of this decad algorithm, we are provided with the K-type of the decad and its relative color off-set, from which, by use of the tables, the true Galois colors of the ten generators is known. The basis set of 4-vectors is provided, hence the full set of the generators becomes known by multiplying on the right by the appropriate matrix, DEC0, or DODEC0T/2. The weights $\boldsymbol{W}$ are provided by the algorithm, as discussed above. A quasi-Gaussian smoothing operation can now be synthesized from the ten sequentially applied line smoothers (also each quasi-Gaussian) where each line smoother's second moment, in units of the generalized grid line along which it is applied, is just the corresponding weight component, W_i, of $\boldsymbol{W}$.

5. Discussion and conclusions

The problem we have addressed is to find a systematic way of generalizing the existing Triad and Hexad algorithms of two and three dimensions to the true Decad algorithm in four dimensions. We have succeeded by exploiting the symmetry properties of the Galois field, $GF(16)$ and its associated finite project geometry, $PG(3,2)$, especially the restricted group of the automorphisms that we have called $\mathrm{Aut}^{+}\{PG(3,2)\}$ that seem best adapted to our problem. The outcome is a reliable algorithm which, given any valid 4D symmetric aspect tensor with its ten independent components, will provide a unique set (the decad) of generalized grid line directions (the integer 4-vector generators). In addition the algorithm supplies precisely the amount (measured by the rank-one projected aspect tensor weight) of Gaussian smoothing that is required to be applied along the space-time grid lines oriented parallel to these generators, in the sequence orchestrated by the different Galois colors, so that the product smoothing operation is the Gaussian convolution with exactly the second moment 'aspect tensor' attribute intended.

The expected application of this method is primarily to a data analysis generalizing what is already being done in the 2D and 3D RTMA (Pondeca et al., 2011), to a new kind of 'nowcasting' analysis in four dimensions covering a period of time too brief to fit well with the use of a costly forecast model initialization and integration. It is envisaged that the 4D covariances of this scheme would be crafted to stretch out along previously anticipated flow trajectories, as well as to possess the usual spatial anisotropies. In this way, without the intervention of an explicit model integration during the analysis period, the information from data collected up to the present could be objectively analyzed in a more temporally consistent way and extrapolated in the most natural way for a short period into the immediate future, with obvious benefits to the operational forecasting community. In this context, we believe that the accomplishment of providing a successful and efficient Decad Algorithm presents a new practical opportunity in the realm of operational objective nowcasting.

Acknowledgments

The author is grateful to Drs. Kristen Bathmann, Manuel Pondeca, and Styliano Flampouris, for their helpful comments.

References

De Pondeca, M. S. F. V., and Coauthors 2011 The Real-Time Mesoscale Analysis at NOAAs National Centers for Environmental Prediction: Current Status and Development. *Wea. Forecasting,* **26,** 593-612.

Fano, G. 1892 Sui postulati fondamentali della geometria proiettiva in uno spazio lineare a un numero qualunque di dimensioni. *Giornale di Matematiche,* **30,** 106–132.

Hayden, C. M., and R. J. Purser 1995 Recursive filter objective analysis of meteorological fields: applications to NESDIS operational processing. *J. Appl. Meteor.,* **34,** 3–15.

Press, W. H., B. P. Flannery, S. A. Teukolsky, and W. T. Vetterling 1989 *Numerical Recipes.* Cambridge University Press, Cambridge, U. K. 702 pp.

Purser, R. J. 2020 A formulation of the Hexad algorithm using the geometry of the Fano projective plane. NOAA/NCEP Office Note 499.

Purser, R. J., and R. McQuigg 1982 A successive correction analysis scheme using recursive numerical filters. Met. O 11 Tech. Note, No. 154, British Meteorological Office. 17 pp.

Purser, R. J., W.-S. Wu, D. F. Parrish, and N. M. Roberts 2003a Numerical aspects of the application of recursive filters to variational statistical analysis. Part I: Spatially homogeneous and isotropic Gaussian covariances. *Mon. Wea. Rev.,* **131,** 1524–1535.

Purser, R. J., W.-S. Wu, D. F. Parrish, and N. M. Roberts 2003b Numerical aspects of the application of recursive filters to variational statistical analysis. Part II: Spatially inhomogeneous and anisotropic general covariances. *Mon. Wea. Rev.,* **131,** 1536–1548.

Veblen, O., and W. H. Bussey 1906 Finite projective geometries. *Trans. Amer. Math. Soc.,* **7,** 241–259.

Wu, W.-S., R. J. Purser, and D. F. Parrish 2002 Three-dimensional variational analysis with spatially inhomogeneous covariances. *Mon. Wea. Rev.,* **130,** 2905–2916.